Non-dimensional scaling of turbulence characteristics and turbulent diffusivity

Non-dimensional scaling of turbulence characteristics and turbulent diffusivity

G.R. McKee, C.C. Petty[a], R.E. Waltz[a], C. Fenzi, R.J. Fonck, J.E. Kinsey[b], T.C. Luce[a], K.H. Burrell[a], D.R. Baker[a], E.J. Doyle[c], X. Garbet[d], R.A. Moyer[e], C.L. Rettig[c], T.L. Rhodes[c], D.W. Ross[f], G.M. Staebler[a], R. Sydora[g], M.R. Wade[h]
University of Wisconsin-Madison,
Madison, Wisconsin,
United States of America

Abstract. Plasma turbulence characteristics, including radial correlation lengths, decorrelation times, amplitude profile and flow velocity, have been measured during a ρ^* scan on DIII-D while all other transport relevant dimensionless quantities (e.g., β, ν^*, κ, q, T_e/T_i) are held nearly constant. The turbulence is measured by examining the correlation properties of the local long wavelength ($k_\perp \rho_i \leq 1$) density fluctuations, measured with beam emission spectroscopy. The radial correlation length of the turbulence $L_{c,r}$ is shown to scale with the local ion gyroradius, $L_{c,r} \approx 5\rho_i$, while the decorrelation times scale with the local acoustic velocity as $\tau_c \sim a/c_s$. The turbulent diffusivity parameter, $D \sim (L_c, r^2/\tau_c)$, scales in a roughly gyro-Bohm-like fashion, as predicted by the gyrokinetic equations governing turbulent transport. The experimental one fluid power balance heat diffusivity scaling and that from GLF23 modelling compare reasonably well.

1. Introduction

Transport of energy and particles across confining magnetic field surfaces is observed in most confinement regimes to be anomalously large, i.e. well above the predictions from binary Coulomb collisions between plasma ions and electrons (neoclassical transport). This anomalous transport is believed to result from turbulence driven largely by pressure gradients. Predicting the magnitude of this anomalous transport in larger experimental devices has been addressed by applying the non-dimensional scaling technique in existing tokamaks [1–5]. A central assumption in the non-dimensional scaling approach is that this anomalous transport is a function of local dimensionless quantities, including β (ratio of plasma to magnetic pressure), q (safety factor), ν^* (collisionality), T_e/T_i, κ (elongation), R/a (aspect ratio), L_n/a, L_T/a (density and temperature gradient scale lengths divided by the minor radius), M (Mach number, $M = v_\phi/c_s$, $c_s = \sqrt{T_e/M_i}$, the sound speed) and ρ^* ($= \rho_i/a$), the ratio of ion gyroradius to plasma minor radius. Existing experimental devices can match all of these transport relevant dimensionless parameters expected in reactor scale devices with the exception of ρ^*; thus the scaling of transport with ρ^* is of central importance.

Significant experimental and theoretical effort has been expended on determining the ρ^* scaling of anomalous transport. Nearly all theories of turbulent transport are inherently gyro-Bohm and thus predict that $\chi \sim \chi_B(\rho^*)^1$, with $\chi_B = \rho_s c_s$. Experiments, however, have shown that transport coefficients can scale in a gyro-Bohm- or Bohm-like fashion, depending on the plasma confinement regime (L or H mode) and the transport channel under investigation [5–7]. The ion channel in L mode plasmas typically exhibits a Bohm- or worse-than-Bohm-like scaling, $\chi_I \sim \chi_B(\rho^*)^0$, as can the global energy confinement scaling. Electron heat transport, in contrast, is always observed to exhibit gyro-Bohm-like scaling. The effective heat diffusivity and global energy confinement scaling can then depend on whether the electron or ion conductivity is dominant.

Previous experimental studies on the non-dimensional scaling of transport have been based largely on the scaling of inferred heat and particle transport coefficients and energy confinement times. Typically, one dimensionless parameter, often ρ^*, is

[a] General Atomics, San Diego, California, USA.
[b] Lehigh University, Bethlehem, Pennsylvania, USA.
[c] University of California, Los Angeles, California, USA.
[d] Association Euratom–CEA sur la Fusion, Cadarache, France.
[e] University of California, San Diego, California, USA.
[f] University of Texas at Austin, Austin, Texas, USA.
[g] University of Alberta, Edmonton, Alberta, Canada.
[h] Oak Ridge National Laboratory, Oak Ridge, Tennessee, USA.

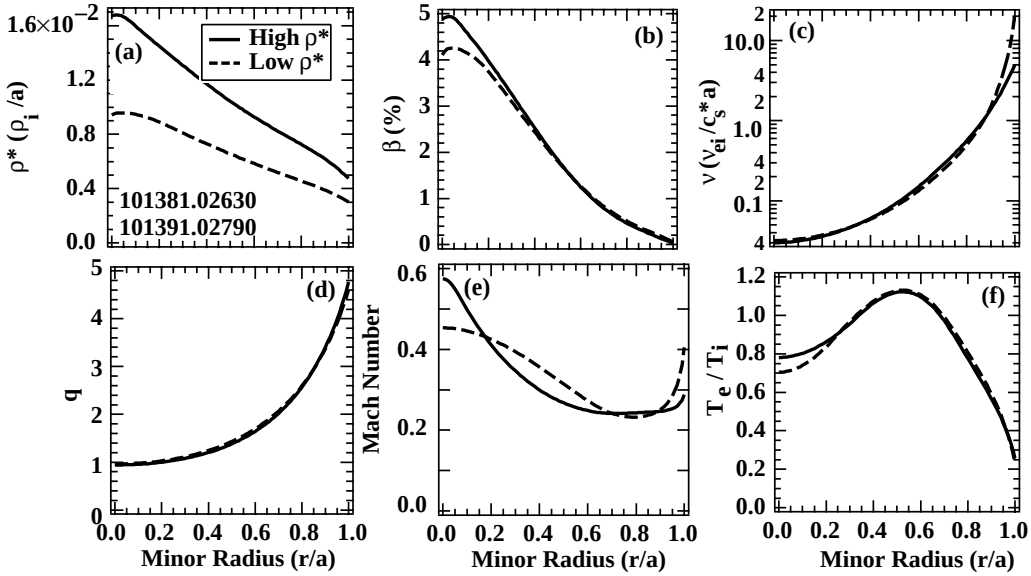

Figure 1. Profiles of (a) ρ^*, (b) beta, (c) collisionality ν, (d) safety factor q, (e) Mach number and (f) T_e/T_i ratio for the dimensionless ρ^* scan. ρ^* is varied by 1.6 while the other quantities are held nearly constant.

varied while other dimensionless quantities are held constant. This study represents the first experiment to systematically measure the scaling characteristics of the underlying turbulence driving the anomalous transport during a non-dimensional ρ^* scan. The goal has been to elucidate the underlying processes, determine the scaling of turbulence characteristics and quantitatively test predictions of the inherently gyro-Bohm-like gyrokinetic equations. These experiments were performed in the DIII-D tokamak, and the turbulence was characterized by measuring density fluctuations with the beam emission spectroscopy diagnostic system [8, 9]. The experiments, fluctuation measurements and modelling are discussed.

2. $\boldsymbol{\rho^\Lambda}$ Scaling experiments

In order to determine the ρ^* scaling of plasma turbulence structures and parameters, plasma discharges with well matched dimensionless quantities (e.g., β, ν^*, q, T_e/T_i, M) were produced while ρ^* was varied. The discharges were elliptical and inner wall limited L mode plasmas. These were chosen to provide relatively quiescent steady state plasma conditions, which are preferable for fluctuation diagnosis. The plasma geometry was maintained constant during the scan with major radius $R_0 = 1.65$ m, minor radius $a = 0.63$ m and elongation $\kappa = 1.54$.

The ρ^* scan was performed by varying the toroidal magnetic field and current (to match q) by a factor of 2, as has been the standard method in previous non-dimensional scaling experiments on DIII-D [6]. Density and heating power are adjusted via gas puffing and neutral beam power as necessary to keep the profiles of all dimensionless parameters, with the exception of ρ^*, constant. The resulting temperature and field variation changes ρ^* by a factor of roughly 1.6 in this scan. The profiles of ρ^*, β, ν^*, q, T_e/T_i and M are shown in Fig. 1, indicating a variation of roughly 1.6 in ρ^*, while the other dimensionless variables are held nearly constant across the plasma profile. A slight mismatch in the Mach number will be discussed in Section 4. The energy confinement time for the high and low ρ^* discharges varies from 47 to 60 ms, and thus exhibited Bohm-like scaling ($\tau_E \propto B^{1/3}$).

The linear gyrokinetic ballooning mode growth rates were calculated for the two discharge conditions in this ρ^* scan to determine if the growth rates are well matched. These calculations were performed with the gyrokinetic simulation (GKS) code [10, 11], including actual plasma geometry. The profiles of the maximum linear growth rates normalized to c_s/a are shown in Fig. 2. The very close match between the two curves shows that the discharges are well matched theoretically since these rates depend on all the dimensionless parameters except ρ^*.

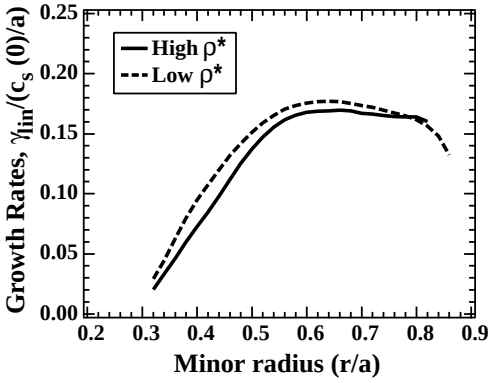

Figure 2. Profiles of the maximum linear growth rate (calculated with the GKS code), normalized to $c_s(0)/a$, in the low and high ρ^* discharges, showing a very close match indicating that the turbulent transport would be expected to be gyro-Bohm-like.

3. Fluctuation parameter scaling

The primary goal of this study was to measure the scaling of the radial correlation length, decorrelation time and amplitude of turbulent eddy structures. Measurements of these fluctuation characteristics, as well as their scaling, were obtained with a beam emission spectroscopy (BES) diagnostic. The BES system measures the local long wavelength ($k_\perp \leq 2.5$ cm^{-1}) density fluctuations at a spatial resolution of $\Delta r \approx 1$ cm. It observes the Doppler shifted neutral beam emission at D_α ($n = 3$ to $n = 2$ at $\lambda \approx 653$ nm) arising from excitation of the beam as it traverses the plasma and collides with the background plasma ions and electrons. Diagnostic details are discussed in Ref. [8]. The long wavelength density fluctuations measured are believed to arise predominantly from electrostatic drift-wave-like turbulence and can transport ions and electrons across the magnetic field via turbulent $\boldsymbol{E} \times \boldsymbol{B}$ diffusion: $\Gamma = \langle \tilde{n}\tilde{v}_r \rangle = \langle \tilde{n}\tilde{E}_\theta / B_T \rangle$.

The BES instrument has 32 spatial channels which were deployed as follows: 14 radially separated channels and two poloidal arrays of eight channels each, with roughly 1 cm separation between the radial and poloidal channels. The set-up is shown in Fig. 3 along with an equilibrium reconstruction of the flux surface shapes. Two channels are situated deeper in the plasma to monitor the common mode fluctuation power [9]. The radially separated channels allow for a measurement of the radial correlation length and fluctuation amplitude profile, while the poloidally separated channels provide measurements of the decorrelation time, poloidal correlation length and poloidal convection velocity of the density fluctuations, all quantities integral to this investigation.

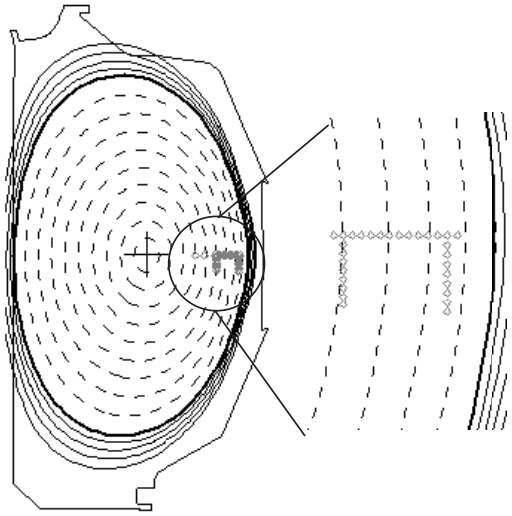

Figure 3. EFIT equilibrium reconstruction showing the locations of the 32 spatial BES channels, with one radial array (14 channels), two poloidal arrays (8 channels each) and two common mode monitoring channels. The array was moved on repeat discharges to scan across the profile.

3.1. Fluctuation amplitude profile

The fluctuation amplitude profiles, shown in Fig. 4(a), indicate that the normalized fluctuation level $\tilde{n}/n$ increases over the entire profile with ρ^*. The profiles show that in both ρ^* conditions the fluctuation amplitude increases rapidly from the core to the edge of the plasma. This presents a practical issue in that measurement of quantities such as correlation lengths and decorrelation times requires a sufficient signal to noise ratio in the fluctuation amplitude. As $\tilde{n}/n$ falls below about 0.5%, the signal to noise ratio becomes too low to confidently measure the quantities. Thus the turbulence characteristics are studied in the radial region $0.7 \leq \rho \leq 1.0$ where a sufficient signal to noise ratio allows for such measurements. The ratio of the fluctuation profiles, $[\tilde{n}/n]_{2\,\mathrm{T}}/[\tilde{n}/n]_{1\,\mathrm{T}}$, is shown in Fig. 4(b), indicating a scaling of roughly $[\tilde{n}/n] \sim (\rho^*)^{1.4\pm0.4}$. Gyro-Bohm based models predict that the fluctuation amplitude should scale as $\tilde{n}/n \sim (\rho^*)^1$ [12]. The radial variation of the $\tilde{n}/n$ ratio shows significant variance and, given the experimental uncertainty, is not inconsistent with the gyro-Bohm predictions.

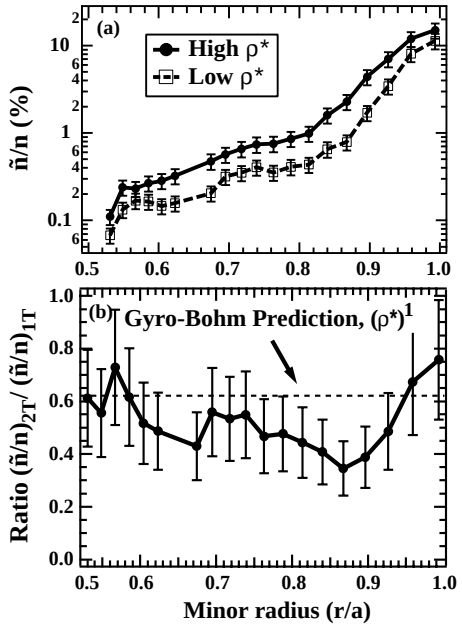

Figure 4. (a) Profile of the normalized density fluctuation amplitude $\tilde{n}/n$ for the two ρ^* discharges, showing a strong radial dependence (note the logarithmic scale); (b) the ratio of the density fluctuation profile along with a line at 0.6 indicating gyro-Bohm-like predictions.

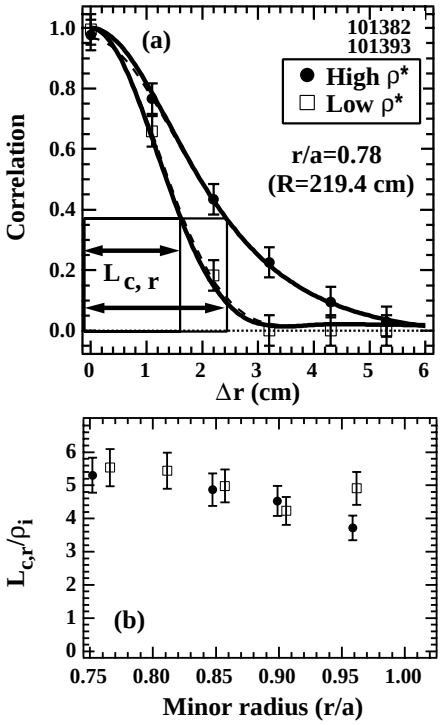

Figure 5. (a) Radial correlation function at $r/a = 0.78$ for the two ρ^* discharges showing a shorter radial correlation length $L_{c,r}$ in the low ρ^* discharge, and (b) the ratio of the radial correlation length profile to the ion gyroradius showing the close scaling of the two ρ^* cases, with $L_{c,r} \approx 5\rho_i$.

3.2. Correlation lengths

Turbulent eddy structure sizes and their ρ^* scaling are a key property of the turbulence, and specific predictions for their magnitude are provided by transport simulations. The BES data provide a direct measure of both the radial and poloidal correlation lengths of the plasma turbulence. These quantities are measured by calculating the ensemble averaged temporal correlation between nearby spatial channels. These correlation lengths are interpreted as average eddy structure sizes in the associated direction (radial or poloidal).

The radial correlation function for the low and high ρ^* conditions at $r/a = 0.78$ are shown in Fig. 5(a). The radial correlation length is taken as the distance over which the correlation has dropped to $1/e$. The finite spatial resolution of the BES diagnostic has been spatially deconvolved from the correlation function. For these discharges, the radial correlation lengths at $r/a = 0.78$ are about 1.6 and 2.4 cm in the low and high ρ^* conditions, respectively. The profiles of the correlation length normalized to the ion gyroradii are shown in Fig. 5(b). The radial correlation lengths scale very closely with the local ion gyroradius in both cases such that $L_{c,r} \approx 5\rho_i$. These measurements demonstrate that the turbulence radial correlation length scales with the local ion gyroradius and not with the system size of the plasma, which is, of course, fixed in these experiments. Thus the correlation lengths appear consistent with gyro-Bohm-like scaling. The poloidal correlation lengths, in contrast, do not scale with ρ^* but are roughly constant as ρ^* is varied and have a magnitude near 3.5–4.5 cm over the radial range investigated. The average eddy shapes thus appear to change with ρ^*, changing from a more poloidally elongated shape at low ρ^* to a less elongated shape at higher ρ^*. In both cases, however, the poloidal correlation length exceeds the radial correlation length.

The radial and poloidal wavenumber spectra are shown in Figs 6(a) and (b). These spectra demonstrate the self-similar nature of the wavenumber spectra and indicate that beyond just the matching of radial correlation lengths, an average parameter of the distribution, the distributions of fluctuation power are similar to each other when plotted as

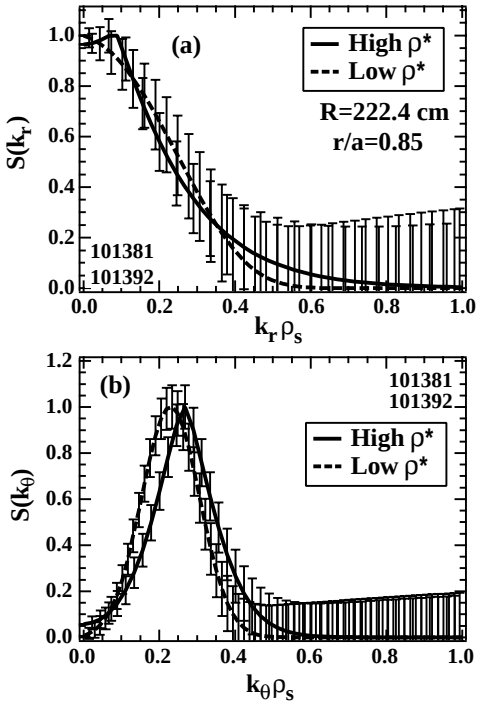

Figure 6. (a) Comparison of the radial wavenumber spectra in the two conditions showing the self-similar nature, and (b) comparison of the poloidal wavenumber spectra. A slight shift is observed, although this is not believed to be correlated directly with cross-field transport.

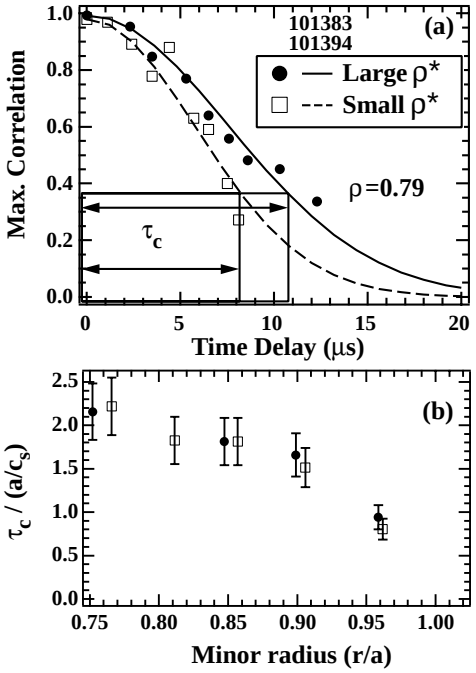

Figure 7. (a) Temporal correlation function of turbulence at $r/a = 0.79$ showing an increase in decorrelation time from $\tau_c \approx 8$ to $\tau_c \approx 11$ μs as ρ^* is increased. (b) Profile of τ_c normalized to a/c_s showing a match between the two conditions, indicating a gyro-Bohm-like scaling.

a function of normalized wavenumber, $k_\perp \rho_s$. There is a slight shift in the poloidal spectrum between the low and high ρ^* conditions which reflects that the average poloidal wavelength does not scale quite as strongly with ρ^* as the average radial wavelength. The radial correlation length is the step size for random walk diffusion and is thus the quantity that is directly relevant to turbulent transport.

The wavenumber spectra are seen to be asymmetric in the radial and poloidal directions, as has been observed previously in tokamak turbulence [13]. The radial wavenumber spectrum peaks at $k_r \rho_s = 0$ indicating no wave-like structure in the radial direction, as expected since there is no radial propagation of turbulent eddies. The poloidal spectrum, in contrast, peaks near $k_\theta \rho_s \approx 0.25$, indicating a wave-like structure. This would be expected given the poloidal propagation observed in the laboratory frame resulting from $\boldsymbol{E} \times \boldsymbol{B}$ and diamagnetic flow. The peak in the poloidal wavenumber spectrum near $k_\theta \rho_s \approx 0.25$ is qualitatively consistent with the predictions of nonlinear gyrokinetic simulations of toroidal ion temperature gradient driven turbulence [14].

3.3. Decorrelation times

Eddy decorrelation times, τ_c, the inverse of the k averaged non-linear growth rate, also interpreted as eddy turnover times, are estimated from the experimental BES data as the decorrelation time of the density fluctuations. This quantity is derived from the ensemble averaged temporal correlation functions of poloidally separated channels. Turbulent eddies are typically advecting uniformly in the poloidal direction at or near the local $E_r \times B$ velocity. We use this aspect to convert poloidal correlation functions to a decorrelation time. Temporal cross-correlation functions are evaluated between a reference channel, which is typically taken at the base of a poloidal array of BES channels. A temporal correlation function is constructed by plotting a graph of the maximum correlation value against the time delay at which the peak occurs for each of the nine channels in a poloidal array [9].

Decorrelation functions for the low and high ρ^* conditions are shown in Fig. 7(a). It is seen that τ_c increases from about 8 μs at low ρ^* to about 11 μs at high ρ^*. Figure 7(b) shows these data correctly normalized to a/c_s, a natural timescale from the

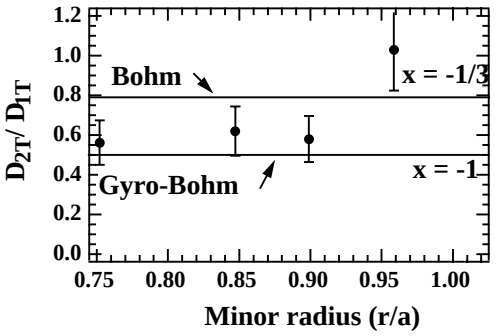

Figure 8. Ratio of the turbulent diffusivity, defined as $D = (L_{c,r})^2/\tau_c$, for the two ρ^* discharges. The profile is most consistent with a gyro-Bohm-like scaling, as expected since both the radial correlation length and the decorrelation time scale in a gyro-Bohm-like fashion. The anomalously large edge point is discussed in the text.

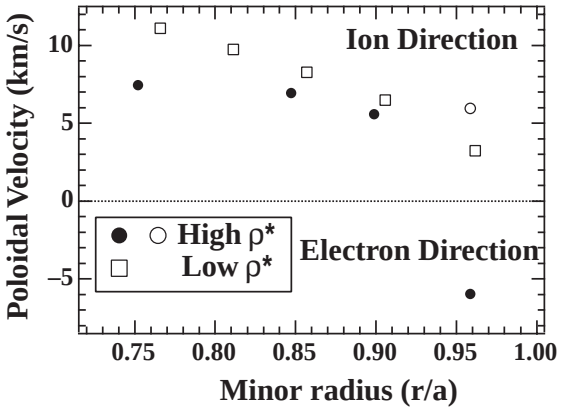

Figure 9. Profile of the poloidal propagation velocity of the turbulent structures as measured in the laboratory frame. For the measurement nearest the edge, two modes are observed in the fluctuation spectra showing an ion and an electron mode, both indicated.

gyrokinetic equations. The striking feature is that with this normalization the two profiles match very well, and have a ratio of the order of unity. There is a slight decrease in this ratio with radius; however, the agreement of these quantities between the two ρ^* conditions suggests that a/c_s is a proper normalizing parameter and that the decorrelation time exhibits a gyro-Bohm-like scaling.

3.4. Turbulent diffusivity scaling

A turbulent diffusivity parameter is constructed from a random walk model of turbulent diffusion, whereby particles are mixed over a radial correlation length on the timescale of the decorrelation time, $D \approx L_{c,r}^2/\tau_c$. The ratio of this diffusivity parameter for the low and high ρ^* conditions, calculated from the above measurements, is shown in Fig. 8, along with the expectations from the Bohm or gyro-Bohm-like scaling laws. Except for the radially outermost point, which appears anomalous, the turbulent diffusivity scaling lies between the Bohm- and gyro-Bohm-like conditions, but closer to the gyro-Bohm-like, as would be expected since both the radial correlation length and the decorrelation times scale in a roughly gyro-Bohm-like fashion. The worse-than-Bohm-like scaling of the edge point (at $r/a = 0.96$) results primarily from the short measured radial correlation length (Fig. 5(b)). The near edge turbulence has a distinctly different character from that of the core turbulence, which is briefly discussed in the next section. It is noted that it is not the absolute magnitude of the diffusion parameter, but rather the scaling of this quantity, that is important for addressing the scaling properties.

3.5. Flow velocity profile

Turbulent structures advect poloidally in the laboratory frame at a velocity that is the sum of the $\boldsymbol{E} \times \boldsymbol{B}$ velocity and a fraction of the ion or electron diamagnetic velocity corresponding to the intrinsic mode phase velocity. Typically the $\boldsymbol{E} \times \boldsymbol{B}$ velocity is much larger than the diamagnetic velocities so that, within the error bars, the $\boldsymbol{E} \times \boldsymbol{B}$ velocity is observed. This velocity is measured experimentally with the poloidal correlation functions discussed in Section 3.3, and is simply $v_{group} = \Delta z/\Delta t$, with Δz the spatial separation and Δt the time delay of the maximum correlation. This is thus a k averaged group velocity, but the phase shift of the poloidal coherency spectra typically shows a linear relation, indicating that all wavenumbers are being uniformly advected in the laboratory frame, or that the derived velocity is nearly the same for all wavenumbers.

The poloidal flow velocity profile is shown in Fig. 9. The fluctuation convection velocity scales closely with the Mach number $M = v_{tor}/c_s$ away from the edge. However, near the edge region, at $r/a \approx 0.96$ in the high ρ^* condition, the fluctuation spectra indicate two distinct modes that are counter-propagating, with low frequency modes travelling in the ion diamagnetic direction, and higher frequency modes propagating in the electron direction. Thus the velocity profile is double valued for high ρ^* at this location. Dual mode edge turbulence has been

observed previously [15] and was interpreted as the observation of distinct electron and ion modes. Here they are presented as characteristics of the edge turbulence, though it is not clear if or how they affect confinement. The radial correlation length at this edge location in the high ρ^* condition was observed to be well below the scaling curve (Fig. 5(b)) for the other channels, suggesting that this edge turbulence has a fundamentally different nature.

4. Modelling predictions and discussion

Turbulent transport simulations of these ρ^* scaling discharges using the GLF23 model [16] were performed to further elucidate these experimental observations. The GLF23 transport model is a nonlinear gyrofluid model that includes the toroidal ion temperature gradient mode, trapped electron drift modes (collisionless and dissipative), ideal MHD ballooning modes, edge resistive modes and electron temperature gradient modes, as well as $\boldsymbol{E}\times\boldsymbol{B}$ shear, magnetic shear and Shafranov shift (α) stabilization mechanisms. The GLF23 simulations indicate that the ratio of the predicted effective thermal diffusivities scale between Bohm and gyro-Bohm for this pair of ρ^* conditions, as shown in Fig. 10. Here we compare the ratio of the effective thermal diffusivities from GLF23 with the single fluid diffusivity inferred from the experimental heat flux. We also include the ratio of the random walk diffusivities obtained from the turbulence measurements. Within their respective uncertainties, they all roughly agree and indicate that the scaling is between gyro-Bohm and Bohm.

The GLF23 transport model is an intrinsically gyro-Bohm model, and so it is important to identify the gyro-Bohm breaking mechanism in the simulation for these discharges. Gyro-Bohm breaking mechanisms may include small but important mismatches in the dimensionless parameter profiles, non-linear coupling of highly unstable short wavelength modes to longer wavelength modes that scale with gradient scale lengths (and therefore system sizes) [17–20], or a diamagnetically driven (ρ^* dependent) $\boldsymbol{E}\times\boldsymbol{B}$ shear reduction of growth rates [21]. GLF23 modelling indicates that a slight mismatch in the Mach number (Fig. 1(e)) may alter the $\boldsymbol{E}\times\boldsymbol{B}$ shear rate and break the intrinsic gyro-Bohm scaling of the transport. The $\boldsymbol{E}\times\boldsymbol{B}$ shearing rate modifies the growth rate, $\gamma_{NET} = \gamma_{lin} - \gamma_{\boldsymbol{E}\times\boldsymbol{B}}$. $\gamma_{\boldsymbol{E}\times\boldsymbol{B}}$ contains both a rotational term and a diamagnetic term. The simulation showed that the diamagnetic term is negligible and so $\gamma_{\boldsymbol{E}\times\boldsymbol{B}}$ is dominated by the toroidal rotation term. Here, $\boldsymbol{E}\times\boldsymbol{B}$ flow shear stabilization effects were found to be more important in the high ρ^* case than in the low ρ^* case. This would then reduce transport in the high ρ^* case, resulting in the scaling being apparently poorer than gyro-Bohm scaling.

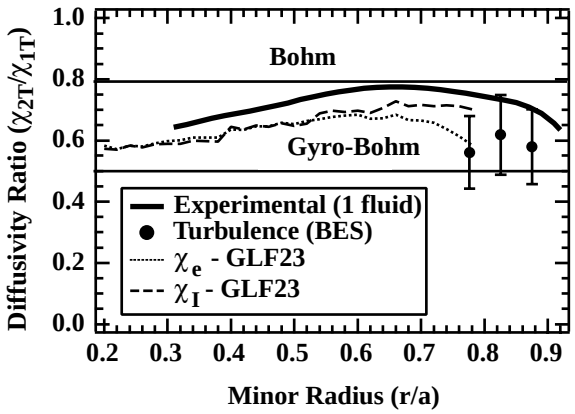

Figure 10. Profiles of the ratio of heat diffusivity for a one fluid power balance, GLF23 simulation, and the fluctuation diffusivity parameter showing reasonable consistency.

We note that with a two fluid power balance analysis applied to these discharges, the electron heat diffusivity χ_e scales in a gyro-Bohm-like fashion while the ion heat diffusivity χ_i scales worse than Bohm-like, as has been seen in past experiments [6]. These recent experimental results do not resolve this issue. Further simulations and experiments are required to understand this observation. Present studies suggest that the worse than Bohm ion diffusivity may be related to the difference between the power balance diffusivity and the incremental diffusivity. Small changes in the critical gradient, induced by slight Mach number mismatches, can lead to large changes in the predicted heat flux, thus allowing for corresponding differences in the scaling characteristics of the incremental and power balance heat diffusivities. This will be investigated in future studies.

5. Conclusion

This experimental study has provided the first direct measurements of the scaling of density fluctuation characteristics during a systematic non-dimensional ρ^* scan. These measurements were obtained with the BES diagnostic in well matched L mode discharges on DIII-D where all the dimen-

sionless parameters, with the exception of ρ^*, were held constant. It has been shown that the turbulence radial correlation lengths scale with the local ion gyro-radius ρ_i and that the decorrelation time τ_c scales with a/c_s. The fluctuation amplitude scales as $\tilde{n}/n \propto (\rho^*)^{1.4\pm0.4}$. These scaling characteristics are in reasonably good agreement with the predictions from gyro-Bohm models of turbulent transport. The turbulent diffusivity parameter ($D \approx L_{c,r}^2/\tau_c$) scales between gyro-Bohm- and Bohm-like, but appears closer to gyro-Bohm-like. Within the uncertainties, this agrees with the single fluid experimental power balance heat diffusivity scaling, and that from the GLF23 modelling.

Acknowledgements

This work has been supported by the US Department of Energy under Grant Nos DE-FG03-96ER54373, DE-FG03-95ER54294 and DE-FG03-86ER53225, and Contract Nos DE-AC03-99ER54463 and DE-AC05-96OR22464.

References

[1] Waltz, R.E., DeBoo, J.C., Rosenbluth, M.N., Phys. Rev. Lett. **65** (1990) 2390.
[2] Connor, J.W., Taylor, J.B., Nucl. Fusion **17** (1977) 1047.
[3] Cordey, J.G., et al., Plasma Phys. Control. Fusion **38** (1996) A67.
[4] Perkins, F.W., et al., Phys. Fluids B **5** (1993) 477.
[5] Petty, C.C., et al., Phys. Rev. Lett. **74** (1995) 1763.
[6] Petty, C.C., et al., Phys. Plasmas **2** (1995) 2342.
[7] Luce, T.C, Petty, C.C., Balet, B., Cordey, J.G., in Plasma Physics and Controlled Nuclear Fusion Research 1996 (Proc. 16th Int. Conf. Montreal, 1996), Vol. 1, IAEA, Vienna (1997) 611.
[8] McKee, G.R., et al., Rev. Sci. Instrum. **70** (1999) 913.
[9] Durst, R.D., et al., Rev. Sci. Instrum. **63** (1992) 4907.
[10] Kotschenreuther, M., et al., Comput. Phys. Commun. **88** (1995) 128.
[11] Waltz, R.E., Miller, R.L., Phys. Plasmas **6** (1999) 4264.
[12] Manfredi, G., Ottaviani, M., Phys. Rev. Lett. **79** (1997) 4190.
[13] Fonck, R.J., et al., Phys. Rev. Lett. **70** (1993) 3736.
[14] Parker, S.E., Lee, W.W., Santoro, R.A., Phys. Rev. Lett. **71** (1993) 2042.
[15] Durst, R.D., et al., Phys. Rev. Lett. **71** (1993) 3135.
[16] Waltz, R.E., et al., Phys. Plasmas **4** (1997) 2482.
[17] Sydora, R.D., Decyk, V.K., Dawson, J.M., Plasma Phys. Control. Fusion **38** (1996) A281.
[18] Biglari, H., Diamond, P.H., Phys. Fluids B **3** (1991) 1797.
[19] Tang, W.M., Rewoldt, G., Phys. Fluids B **5** (1993) 2451.
[20] Furnish, G., et al., Phys. Plasmas **4** (1997) 169.
[21] Garbet, X., Waltz, R.E., Phys. Plasmas **3** (1996) 1898.

(Manuscript received 4 October 2000
Final manuscript accepted 2 May 2001)

E-mail address of G.R. McKee:
mckee@fusion.gat.com

Subject classification: D2, Te; F2, Te